Scanning Microscopy Vol. 11, 1997 (Pages 427-436) 0891-7035/97$5.00+.25
Scanning Microscopy International, Chicago (AMF O'Hare), IL 60666 USA

ANALYSIS AND SIMULATION OF DIGITAL ELECTRON HOLOGRAMS FROM POLYMER LATEXES

Y.C. Wang, T.M. Chou and M. Libera*

Department of Chemical, Biochemical and Materials Engineering, Stevens Institute of Technology, Hoboken, NJ

Abstract

This paper describes procedures being developed to quantitatively measure mean inner potential, Φ_o, and use such data in holographic image simulations of polymer microstructure. Results from holographic imaging experiments are presented using polymer latexes whose spherical geometry leads to a simple relation between specimen thickness and lateral position in a phase image. Success with this approach demands accurate determination of the center and radius in the image of a latex sphere. These parameters are found via a least-squares fit to experimental image data. Recursive methods to enhance the accuracy of the measured Φ_o values are being developed based on characteristic features in difference images generated using an experimental phase image and a simulated phase image calculated from experimentally-derived center, radius, and Φ_o data.

Key Words: Latex sphere, multi-phase polymer microstructure, styrene-butadiene-styrene triblock copolymer, transmission electron holography, phase-contrast imaging, electron-optical refractive index, mean inner potential, simulation of phase image, least-squares fit, spherical geometry.

*Address for correspondence:
Matthew Libera
Department of Chemical, Biochemical and Materials Engineering, Stevens Institute of Technology,
Hoboken, NJ 07030

Telephone number: (201) 216-5259
FAX number: (201) 216-8306
E-mail: mlibera@attila.stevens-tech.edu

Introduction

Transmission electron microscopy (TEM) has been used extensively over the past few decades as a tool to measure polymer microstructure. The principal TEM imaging method employed for the study of multiphase amorphous or semicrystalline polymers uses heavy-element stains to preferentially label or decorate one particular polymer phase (Sawyer and Grubb, 1987). Stained regions scatter electrons more strongly than unstained regions. Strongly scattered electrons can be blocked by an objective aperture to induce contrast by changing the electron-wave amplitude contributing to the various parts of an image. Figure 1 shows a typical result. The specimen is a solution-cast film of polystyrene-polybutadiene-polystyrene (SBS) tri-block copolymer. No stain was used to generate the image in Figure 1a, and there is little discernible contrast. Figure 1b shows a similar specimen after being exposed to OsO_4 vapor. OsO_4 reacts preferentially with the unsaturated carbon-carbon double bond in the polybutadiene and gives it dark contrast in a traditional bright-field image.

The rich microphase-separated microstructure evident in figure 1b is present in the unstained specimen of Figure 1a, but there is insufficient differential scattering to resolve the two phases by traditional amplitude-contrast TEM methods. Handlin and Thomas (1983) have shown, however, that phase contrast can be induced in unstained specimens from this same polymer system by defocusing. The phase of an electron wave is modulated by the refractive properties of the specimen, and, if the refractive indices characterizing two different polymer phases are sufficiently different, then image contrast can be generated by mapping the modulated electron wave phase as a function of position in a specimen.

The electron-optical index of refraction, n_{eo}, is related to the distribution of electrostatic potential in a material. Particularly in the case of an amorphous material where orientation-dependent electron channeling effects are minimized, the electrostatic potential can be represented by its mean value known as the mean inner potential Φ_o. Ignoring dynamical scattering effects, the phase shift of an electron wave can be then modeled as:

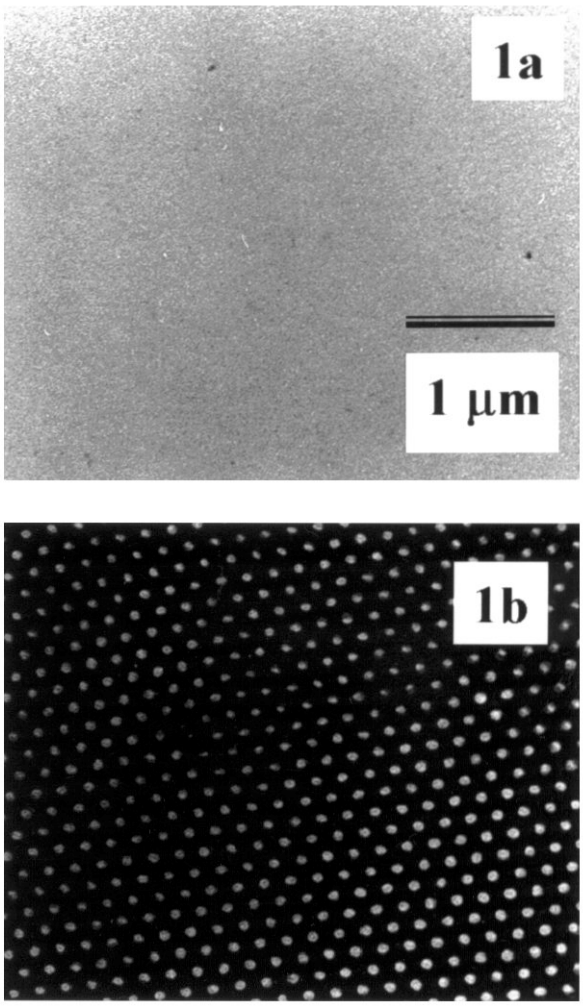

Figure 1. Bright-field image of (**a**) unstained, and (**b**) OsO_4-stained polystyrene-polybutadiene-polystyrene (SBS) polymer thin film.

$$\Delta\varphi = (1/C_E)\Phi_o t \quad \text{or} \quad \Phi_o = C_E\, d\,(\Delta\varphi)/dt \qquad (1)$$

where t is the specimen thickness and C_E is a constant determined by the accelerating potential of the microscope (Landau and Lifshitz, 1965; Gajdardziska-Josifovska *et al*., 1993). While Φ_o values have been measured for a number of inorganic materials (O'Keeffe and Spence, 1994; Saldin and Spence, 1994) and can be estimated using density and atomic-scattering factor data (Rez *et al*., 1994), values characterizing various polymers are not known. Despite the fact that they are principally hydrocarbons, one can anticipate variations in Φ_o that would lead to phase contrast due to differences in density, composition, and the redistribution of valence electron charge due to various possible bonding configurations available to organic materials (Libera *et al*., 1995).

Transmission electron holographic techniques (Lichte, 1991; Tonomura *et al*., 1995) now becoming increasingly practiced throughout the world offer an alternative means to defocus for phase-contrast imaging. Holography measures the phase shift induced by refraction in a specimen relative to an unmodulated reference wave. Reconstruction of a hologram can recover the entire exit-face electron wave function $\iota(x,y) = A(x,y)\exp[-i\phi(x,y)]$ from which either amplitude images ($A(x,y)$) or phase images ($\phi(x,y)$) can be generated. Traditional imaging recovers only the intensity distribution $I(x,y) = |\iota(x,y)|^2$. The potential of holographic techniques to do phase-contrast imaging of unstained polymers is illustrated by figure 2. This shows the result of a simulation assuming a specimen which acts as a pure phase object and has a two-phase lamellar microstructure. The two polymer phases are characterized by mean inner potential values of $\Phi_o^A = 8V$ and $\Phi_o^B = 6V$. Figure 2a shows a simulated hologram with fringe shifts due to differential refraction in the specimen. Reconstruction generates the amplitude and phase images of Figures 2b and 2c, respectively. There is little contrast in the amplitude image as one would expect from a pure phase object. The contrast associated with edge and lamellar interfaces is due to cut-off effects in Fourier space during reconstruction. The phase image shows substantial contrast which faithfully represents the intrinsic structure of this specimen.

Because little is known about the refractive properties characterizing various polymers, we have developed methods based on holographic phase imaging to measure Φ_o values in relevant polymer systems. As indicated by equation [1], Φ_o can be determined if $\Delta\phi$ can be measured from a specimen with a well-known thickness t. Recent work by Gajdardziska-Josifovska *et al*. (1993) and McCartney and Gajdardziska-Josifovska (1994) has exploited wedge and cube-shaped specimens of such materials as Si, GaAs, PbS, and MgO where a functional relation between specimen thickness and lateral position in a phase image can be developed. Our work concentrates on spherical specimens for the same reason (Wang and Libera, 1996; Wang *et al*., 1996). A relation between thickness and lateral position can be developed by knowing the center and radius of a sphere in its projected image. Errors in identifying the projected sphere center and radius lead to errors in the measured Φ_o value. The present paper describes the digital imaging and analysis procedures used to determine Φ_o from spherical polymer latexes and introduces the idea of recursive improvement in the accuracy and precision of these measurements by analysis of characteristic features in difference images formed from experimental and simulated image data.

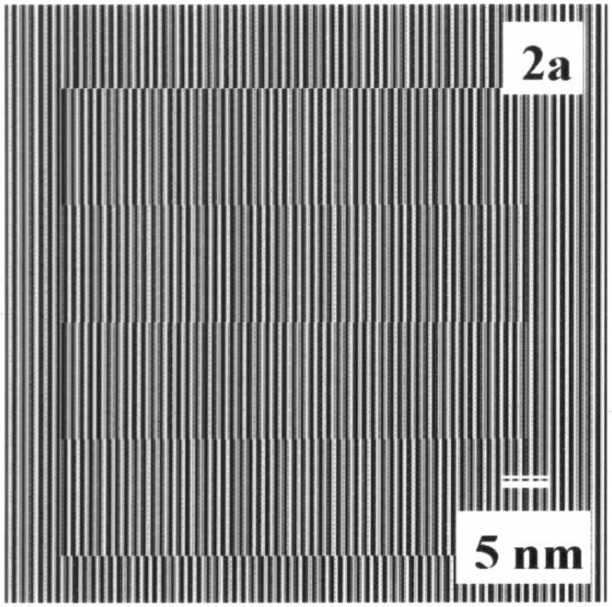

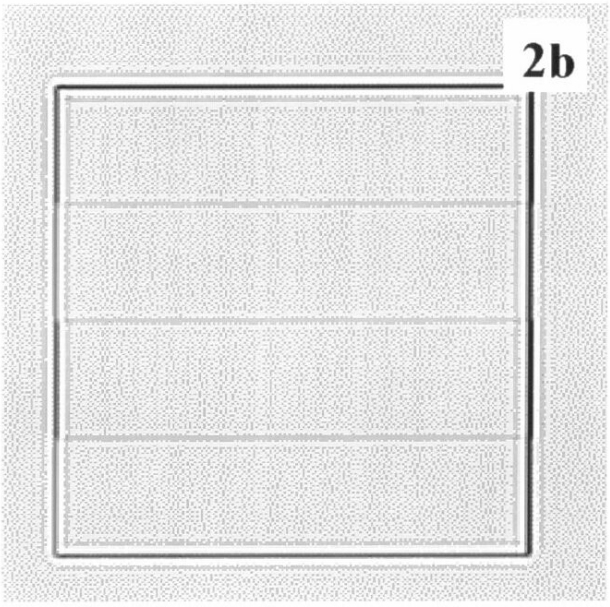

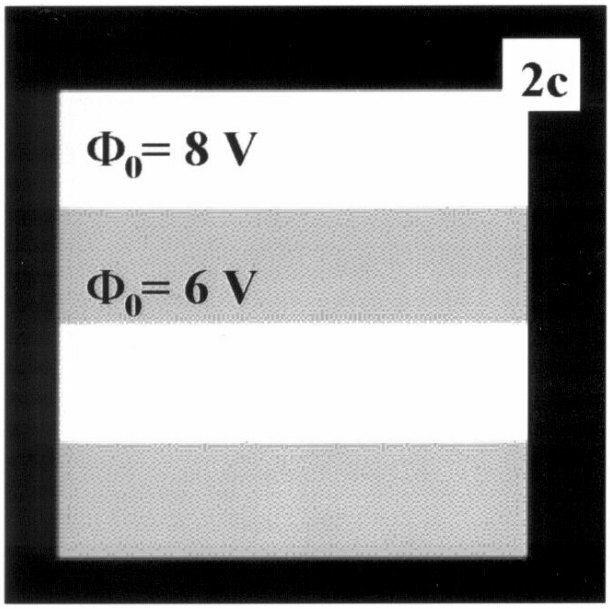

Figure 2. (**a**) simulated hologram of a two-phase lamellar morphology with reconstructed (**b**) amplitude, and (**c**) phase images.

Experimental Methods

Holograms were collected using a 200 keV Philips (Eindhoven, The Netherlands) CM20 TEM/STEM equipped with a Schottky field emitter. The nominal C_E value is 136.77 (nm)(Volt)/(rad). The selected-area aperture mechanism was modified to accommodate a non-rotatable electron biprism (Möllenstedt and Düker 1956; Libera *et al*., 1995). Digital 1024x1024 holograms of polystyrene latex particles were collected with empty reference holograms using a Gatan (Pleasanton, CA) 794 Multiscan camera system. These were reconstructed using the HoloWorks version 1.0 software package developed at Oak Ridge National Laboratory (Voelkl *et al*., 1995). Simulated holograms of latexes were generated assuming kinematic scattering by spherically-shaped pure phase objects characterized by well-defined Φ_o values. Simulations used parameters to give a fringe spacing and pixel resolution comparable to the experimental holograms. Simulated holograms were reconstructed identically as the experimental holograms. Images were manipulated using Digital Micrograph software from Gatan, Inc.

Results and Discussion

An electron hologram of a single polystyrene (PS) latex particle and its reconstructed phase image are presented in Figures 3a and 3b, respectively. The phase image can be used to derive a value for Φ_o^{PS} if the specimen thickness can be established at each pixel. Since the particle has a spherical shape, the thickness t is simply related to the lateral coordinates x and y by:

$$t = 2[R_o^2 - (x-x_o)^2 - (y-y_o)^2]^{1/2} \quad (2)$$

where (x_o,y_o) defines the center of the particle in the phase image and R_o defines its radius. The three parameters x_o, y_o, and R_o must be determined from the experimental data. We have derived these by identifying the set of pixels that best

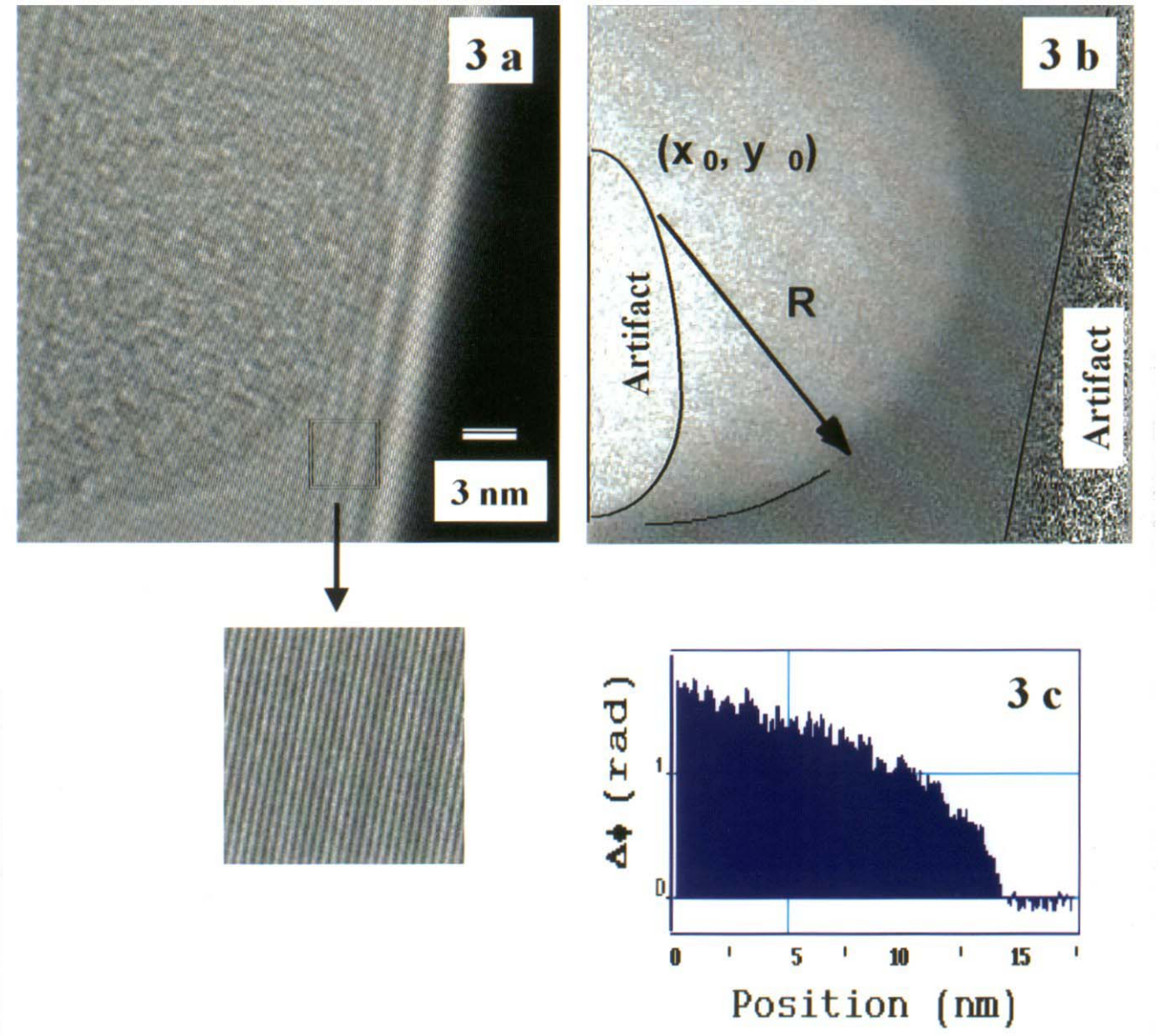

Figure 3. (**a**) experimental hologram of a ~30nm diameter polystyrene latex particle (enlarged inset), (**b**) reconstructed phase image with best-fit edge, center, and radius indicated, (**c**) ten-pixel-averaged line profile from box indicated in (**b**).

defines the edge of the particle in the phase image and then performing a least-squares fit. The three-parameter fit is typically done to a dataset of edge pixels containing hundreds of data points.

Figure 3b shows the result of the edge and center-finding operation with the best-fit circle outlined. Figure 3c shows a line profile of phase shift as a function of radial position for the rectangular box indicated on Figure 3b. The profile is averaged over a ten-pixel width. While sufficiently accurate for most of the radial distance, this averaging process introduces error near the center. We are exploring a representation of the x-y data in radial coordinates but are currently minimizing the error by simply omitting a small portion of the radial phase profiles near the particle's center from subsequent processing steps.

Using Equation (2), the radial coordinate in a phase profile such as that in Figure 3c can be converted to a measure of specimen thickness. One such result is shown in Figure 4. The phase data are no longer equally spaced in this thickness representation because of the nonlinear dependence of thickness on radial position (eqn. 2). As a consequence, there is a greater concentration of data points

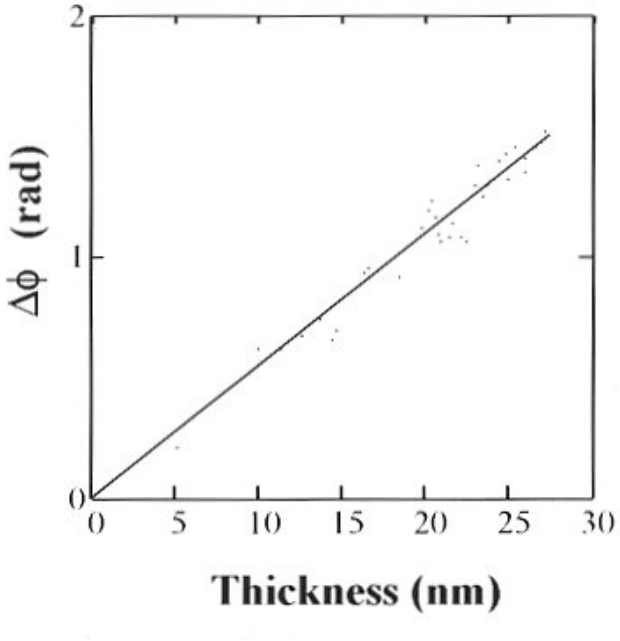

Figure 4. Phase shift as a function of particle thickness from the line profile of Figure 3c.

near the particle center than near the edge. In the thickness representation, the phase-shift data points fall nicely along a straight line. A least-squares fit gives a value for the slope which can be used in Equation (1) to determine Φ_o^{PS}. This particular dataset gives $\Phi_o^{PS} = 7.4V \pm 0.1$ V.

Analysis of results from a number of different latex particles gives a range of Φ_o^{PS} values with an average of 8.2V ± 0.9V. The precision of this experimental measurement needs to be improved in order to demonstrate anticipated differences between various polymers. Possible sources of error are: (i) errors in the reconstruction and analysis process; (ii) the presence of a surfactant layer on each latex particle; (iii) specimen charging; or (iv) error in determining the center and radius of the latex particle in its phase image. Tests of the reconstruction and analysis procedure have been done using simulated holograms whose center, radius, and mean inner potential are all specified. Φ_o, x_o, y_o, and R_o values are recovered which agree to within 1% of the input values indicating that the processing algorithm is sound. The presence of a surfactant layer can be identified by characteristic features in the $\Delta\phi$ vs. t plot (Wang *et al*., 1996) which are absent here. While continued work is needed to fully understand charging effects (Matteucci *et al*., 1988), the characteristic phase shifts in the vacuum due to a net electrostatic charge in the latex particle itself which are consistently observed and studied in large (~1μm diameter) latex particles (Frost *et al*., 1995) have not been observed in our work on sub-50nm diameter particles. This observation raises interesting questions concerning the size dependence of specimen charging in latex particles but will not be further addressed here.

Simulations show that errors in correctly identifying x_o, y_o, and R_o can lead to errors in the determination of Φ_o. A 10% error, for example, in the coordinates of the center produces an equally great error in Φ_o. Error in determining the center and radius comes from inaccurate identification of the image pixels which correspond to the particle edge. Traditional edge-detection operators such as the Roberts or Sobel operators (Russ, 1994; Tovey *et al*., 1995) give clear and unambiguous results when applied to noise-free simulated images but are far less effective when applied to noisy experimental data. Figure 5, for example, shows the result of applying an 11x11 Sobel operator to a model image and an experimental image. The line profiles show that the edge is clearly delineated in the model data but much more poorly in the experimental data. Integrating over a 20 pixel width (Fig. 5e) helps mitigate this problem, but a more-accurate radial average would demand *a priori* knowledge of the particle's center.

We are currently exploring the possibility of using a recursive method to refine the determination of the particle center and radius. The data derived from an experimental phase image are x_o, y_o, R_o, and Φ_o, and these can be used to define a model specimen in a holographic simulation from which a calculated phase image can be derived. Figure 6 shows a calculated phase image using the four data parameters derived from the experimental image of figure 3b. Figure 7 shows a difference image formed by subtracting the calculated phase image (figure 6) from the experimental phase image (Fig. 3b). There is relatively little contrast in the difference image suggesting that the experimentally derived dataset (x_o, y_o, R_o, and Φ_o) is a good one.

Further analysis of the difference image may provide a means for recursive improvement in the determination of the center and radius to enhance the precision with which a Φ_o measurement can be made using a spherical specimen. Characteristic features can be observed when there is not precise agreement between the experimental and calculated phase images. Figure 8 illustrates one possible effect using two calculated phase images where the center of one is offset slightly in the vertical direction relative to the other. A line profile taken along the horizontal direction shows relatively small deviation from zero across its length. The profile along the vertical direction shows a significant deviation from zero at the edge of the sphere. Different features in such perpendicular line profiles can be used to identify the type of discrepancy between the two images. They suggest a direction and magnitude in which x_o, y_o, or R_o could be adjusted to improve the agreement between the two images and, in comparisons between experimental and

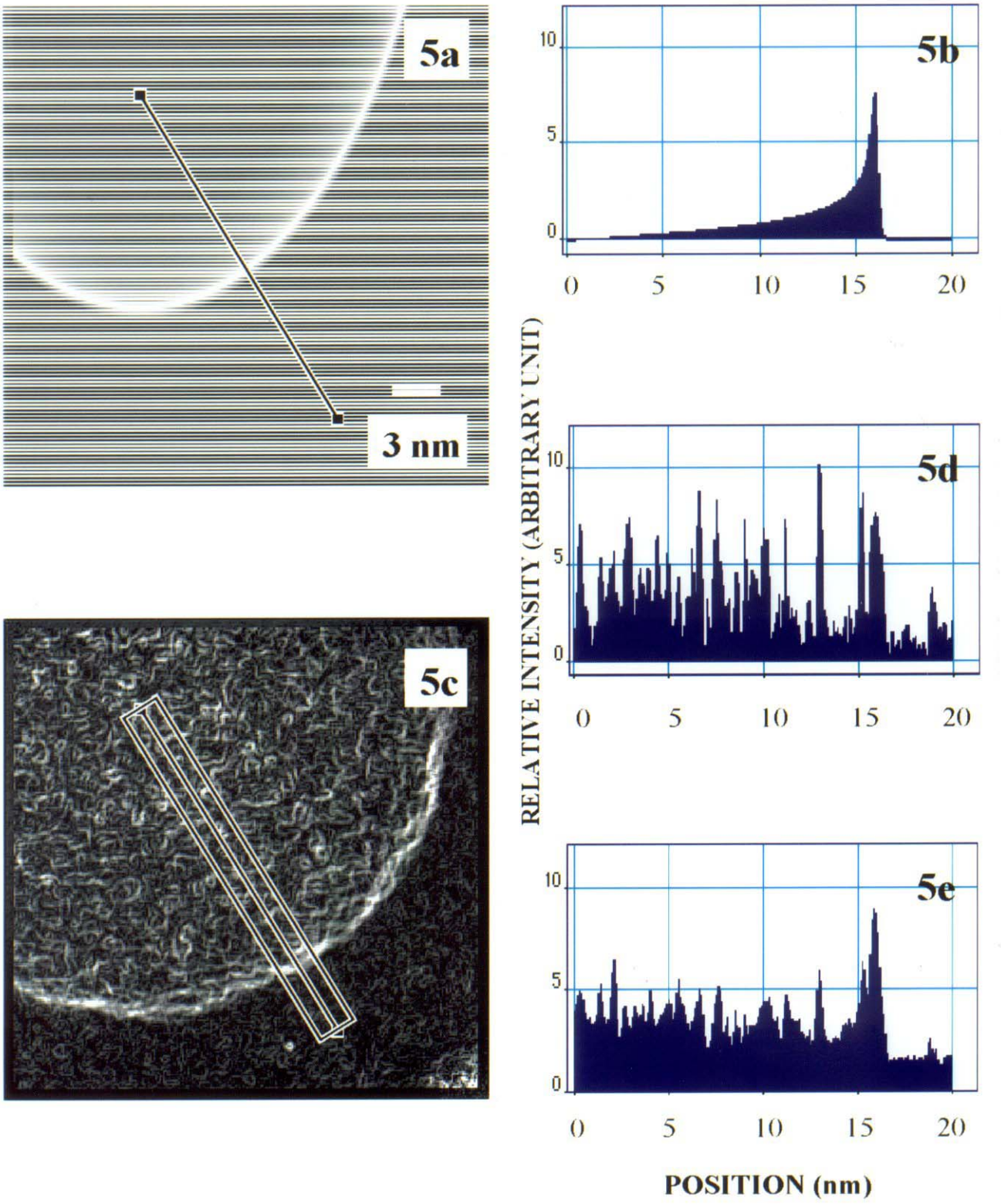

Figure 5. Phase images after application of an 11x11 Sobel edge-finding algorithm (**a**) from simulated holographic phase image with (**b**) 1-pixel wide line profile, and (**c**) from experimental holographic phase image with (**d**) 1-pixel and (**e**) 20-pixel wide line profile.

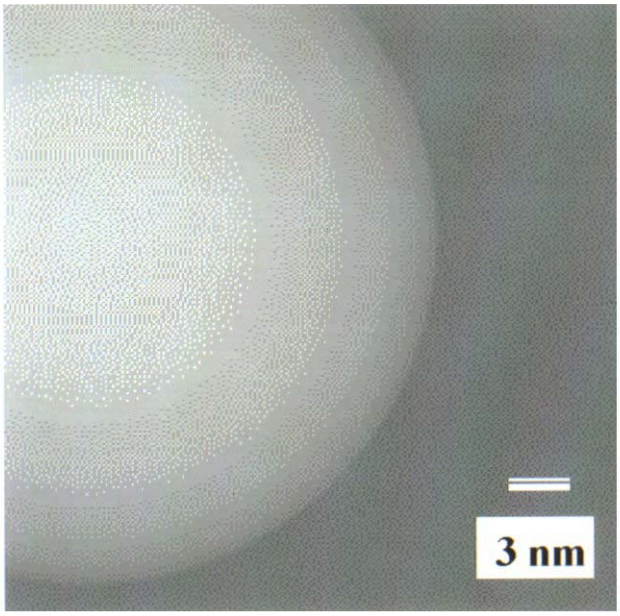

Figure 6. Phase image derived from a holographic simulation using x_o, y_o, R_o, and Φ_o values determined from the experimental data of Figure 3.

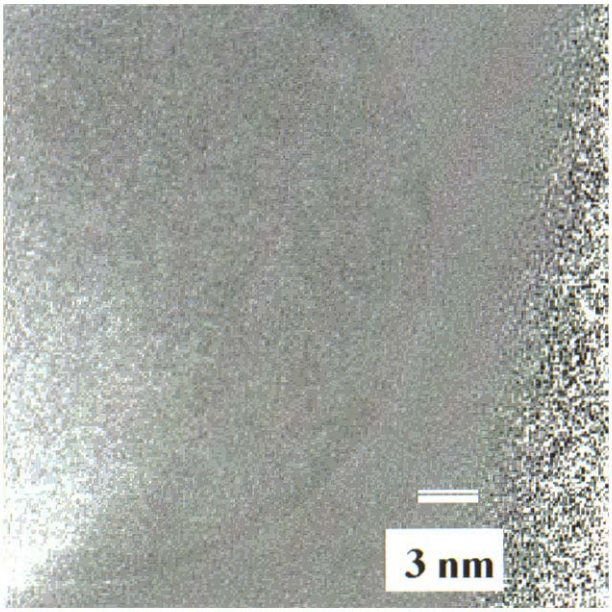

Figure 7. Difference image between the experimental (Fig. 3b) and simulated (Fig. 7) images.

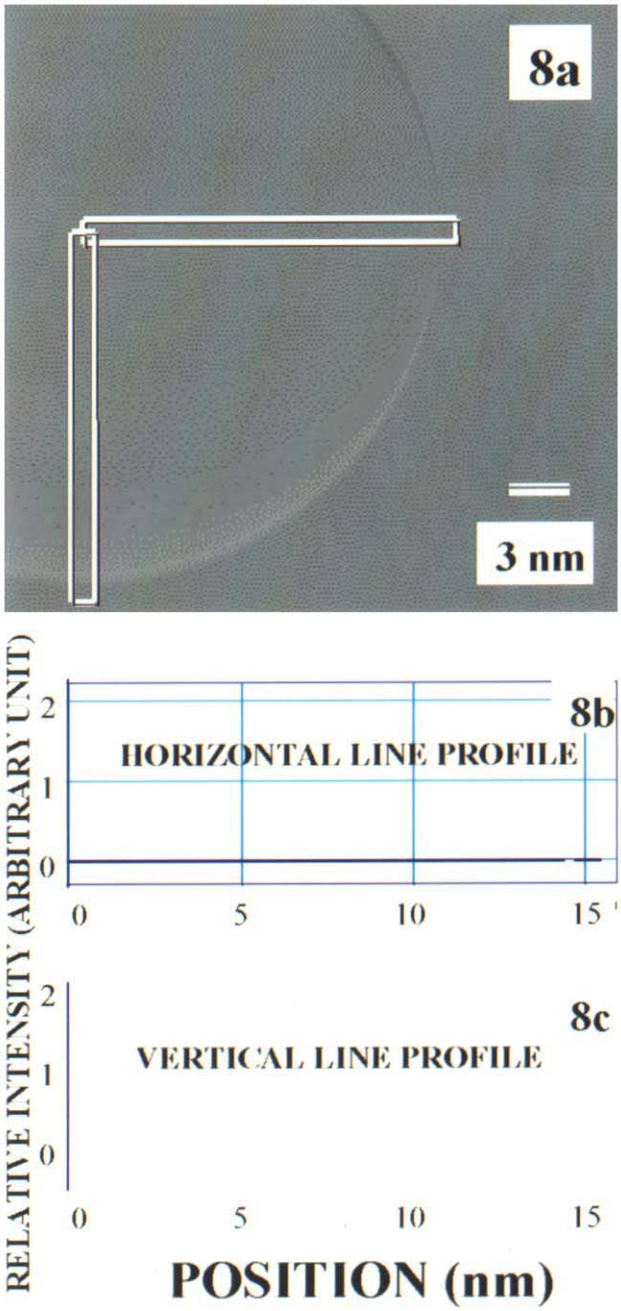

Figure 8. (**a**) Difference image between two identical simulated images offset vertically 0.5nm, (**b**) horizontal line profile, (**c**) vertical line profile.

calculated phase images, lead to more accurate and more precise determinations of Φ_o.

Conclusions

(1) Phase images from latex spheres have been used to make quantitative measurements of the mean inner potential characterizing polystyrene. An average from 15 different experiments gives $\Phi_o^{PS} = 8.2V \pm 0.9$ V.

(2) The relation between specimen thickness and lateral position in a phase image of a latex sphere is essential to these measurements and can be established knowing the center (x_o, y_o) and radius (R_o) of the sphere in its projected image. These parameters were determined by a multi-variable least-squares fit of a circle to a large number of data points in the image defining the sphere edge.

(3) The accuracy with which the least-squares algorithm establishes the thickness-lateral position relationship can be assessed via difference images between simulated and experimental phase images. Recursive methods to improve the accuracy based on such difference methods are being developed.

Acknowledgments

This work is supported by the Army Research Office (grant # DAAH04-93-G-0239) and uses instrumentation jointly funded by the National Science Foundation and the New Jersey Commission on Science and Technology. The authors also thank Olga Shaffer and Victoria Demonie of the Emulsion Polymers Institute at Lehigh Unversity for providing the polystyrene latexes and generous help throughout this work.

References

Frost B, Allard LF, Voelkl E, Joy DC (1995) Holography of electrostatic fields. In: Electron Holography. Tonomura A, Allard L, Pozzi G, Joy D, Ono Y (eds). North Holland, Amsterdam. pp 169-179.

Gajdardziska-Josifovska M, McCartney M, de Ruiter W, Smith DJ, Weiss JK, Zuo J (1993) Accurate measurements of mean inner potential of crystal wedges using digital electron holograms. Ultramicroscopy **50**: 285-299.

Handlin DL, Thomas EL (1983) Phase contrast imaging of styrene-isoprene and styrene-butadiene block copolymers. Macromolecules **16**: 1514-1525.

Landau LD, Lifshitz EM (1965) Quantum Mechanics: Non Relativistic Theory. Pergamon Press, Oxford, UK.

Libera M, Ott J, Wang YC (1995) Transmission electron holography of polymer microstructure. In: Electron Holography. Tonomura A, Allard L, Pozzi G, Joy D, Ono Y (eds). North Holland, Amsterdam. pp 231-238.

Lichte H (1991) Electron image plane off-axis holography of atomic structures. Adv Optical Electron Microsc **12**: 25-91.

Matteucci G, Missiroli GF, Chen JW, Pozzi G (1988) Mapping of microelectric and magnetic fields with double-exposure electron holography. Appl Phys Lett **52**: 176-178.

McCartney M, Gajdardziska-Josifovska M (1994) Absolute measurement of normalized thickness, $t/\ddot{e}_i$, from off-axis electron holography. Ultramicroscopy **53**: 283-289.

Möllenstedt G, Düker H (1956) Beobachtung und Messungen an Biprisma-Interferezen mit Elektronenwellen (Observations and measurements on biprism interferences with electron waves). Z Phys **145**: 377-397.

O'Keeffe M, Spence JCH (1994) On the average coulomb potential and constraints on the electron density in crystals. Acta Cryst **A50**: 33-45.

Rez D, Rez P, Grant I (1994) Dirac-Fock calculations of X-ray scattering factors and contributions to the mean inner potential for electron scattering. Acta Cryst **A50**: 481-497.

Russ JC (1994) The Image Processing Handbook, 2nd edition, CRC Press, Boca Raton. pp 237-249.

Saldin DK, Spence JCH (1994) 0n the mean inner potential in high- and low-energy electron diffraction. Ultramicroscopy **55**: 397-406.

Sawyer LC, Grubb DT (1987) Polymer Microscopy, Chapman and Hall, London. pp 102-122.

Tovey NK, Hounslow MW, Wang J (1995) Orientation analysis and its applications in image analysis. Adv Imaging Electron Phys **93**: 219-329.

Tonomura A, Allard L, Pozzi G, Joy DC, Ono Y (1995) Electron Holography. Elsevier, Amsterdam.

Voelkl E, Allard LF, Frost B (1995) A software package for the processing and reconstruction of electron holograms. J Microsc **180**: 39-50.

Wang YC, Libera M (1996) Mean inner potential measurements of polymer latexes by transmission electron holography. In: Microscopy and Microanalysis 1996. Bailey GW, Dimlich RVW, McCarthy JJ, Pretlow TP (eds). San Francisco Press, San Francisco. pp 168-169.

Wang YC, Chou TM, Libera M, Kelly TF (1996) Transmission electron holography of silicon nanospheres with surface oxide layers. Appl Phys Lett **97**: 1296-1298.

Discussion with Reviewers

D.J. Smith: For typical experimental conditions, such as used for Figure 5c, what was the holographic fringe contrast?
Authors: Figure 5c is an experimental phase image after application of an 11X11 Sobel edge-finding algorithm. The holographic fringe contrast of the original recorded hologram is 14%. This fringe contrast is typical of our holograms.

D.J. Smith: Did the authors undertake any systematic study of fringe contrast vs. image magnification, and thus document its overall effect on image quality (signal-to-noise)?
Authors: No, we did not systematically study the relation between fringe contrast and magnification. In general, the holograms taken at Stevens were collected at 300-400kX and those taken at Oak Ridge National laboratory (ORNL) were collected at 700kX. The poorest phase resolution we found in these holograms is $\pi/20$ measured from the vacuum. Most of the holograms had a phase resolution of order $\pi/40$.

T. Tanji: I do not understand why the averaging error is introduced near the particle center. The ratio of the thickness change over the averaging area is maximum at the edge. And how do you omit the radial phase profiles? Can this problem be solved by considering a particle shape?
Authors: The center is the thickest portion of a sphere. The averaging error of the rectangular box of the line plot near the sphere center is higher compared to the error close to the edge. That is, the weighting percentage of a rectangular box is lower for the center portion than the edge. From the plot of $\Delta\phi$ vs. radial distance, we can easily exclude the digitized data points near the central region. We have considered the object as a particle shape. Then, the $\Delta\phi$ vs. radial distance plot can be converted to the $\Delta\phi$ vs. thickness plot by knowing the center/radius of the spherical object.

T. Tanji: How much in radian is the maximum difference evaluated from Figure 7? And how much does it affect to mean inner potential obtained?
Authors: Since the recorded experimental phase image is pretty noisy and carries artifacts, the maximum difference in Figure 7 has no influence on the determination of mean inner potential. By the way, the radian difference inside the object of Figure 7 can be related to a statistical parameter χ^2 and used for finding the best center/radius/mean inner potential fit of a spherical shape object.

T. Tanji: The explanation of Figure 2 should include data besides inner potentials, e.g., an accelerating voltage, a defocus value, a coefficient of a spherical aberration etc. Phase contrast might be observed under a suitable defocusing.
Authors: We assumed that the simulated hologram and its reconstructed phase image are focused and ignored the transfer property of the microscope.

T. Tanji: In our experiment electron charge accumulated in the latex sphere of 0.5 micron in diameter has been analyzed 6E-17 Coulomb. Of course the amount of charge depends experimental conditions, but we may guess the charge in the sphere of 50 nm in diameter is a few electrons, which may be difficult to be detected by means of an ordinary experiment.
Authors: The charging problem of ~50 nm PS spheres is checked by the line plot in the vacuum region of the experimental phase image and a simulated phase image of $1X10^{-9}$ Coulomb charged sphere. We have not found any evidence of charging effect. On the other hand, we have collected some low-magnification holograms where the field of view is larger but where the phase resolution is smaller than in high-magnification holograms. We still see no evidence of charging in these low-magnification holograms. The amount of static charge on these particles is either too small for us to detect or is being drained to ground due to the small particle sizes (typically 30nm $\rightarrow$ 100nm) we are studying.

J. Bonevich: The authors should use the standard mathematical notation in their equations. For example, in Equation (1) the symbol Φ_0 is used for the mean inner potential, whereas V_0 or U_0 is typically employed. The symbol Φ is commonly taken to be the phase of the electron wave. This is a very minor revision, but serves to make the paper consistent with the literature.
Authors: We used $\Delta\phi$ for the phase shift and Φ_0 for the mean inner potential. This is consistent with papers by John Spence and coworkers as well as other papers we have published previously.

G. Matteucci: The interference field width is not given explicitly. However, from the figures it seems that the authors could try to obtain phase difference amplified maps on the whole sphere so as to observe a map of the thickness variations to obtain an indication of the sphericity together with a somewhat more comprehensive approach for the determination of the sphere center. How did they check that the spheres did not charge significantly?
Authors: The sphericity of the latex particle is a legitimate concern. The polymers we have studied are amorphous and have a T_g well above room temperature. We would not expect these to facet because of isotropic surface energy or mechanically deform by viscous flow during the experiment. The response for the charging problem is same as the response for Dr. Tanji.

G. Matteucci: It would be better to report, in the inset of Figure 3a, the fringes through the sphere since those outside are unimportant for the required phase detection.
Authors: The inset of Figure 3a just simply shows the magnified interference fringes. The point is really just to show that fringes are present, since they are difficult to see in the lower magnification hologram. Since the latex sphere

imparts only a small and smoothly varying phase shift on the incident wave, the fringes from the specimen look much like those in vacuum except with more noise.